Fully nonlinear phenomenology of the Berk–Breizman augmentation of the Vlasov–Maxwell system

R. G. L. Vann, R. O. Dendy, G. Rowlands, T. D. Arber, and N. d'Ambrumenil

Citation: Phys. Plasmas **10**, 623 (2003); doi: 10.1063/1.1539854
View online: http://dx.doi.org/10.1063/1.1539854
View Table of Contents: http://pop.aip.org/resource/1/PHPAEN/v10/i3
Published by the American Institute of Physics.

Fully nonlinear phenomenology of the Berk–Breizman augmentation of the Vlasov–Maxwell system

R. G. L. Vann
Department of Physics, University of Warwick, Coventry CV4 7AL, United Kingdom

R. O. Dendy[a)]
Department of Physics, University of Warwick, Coventry CV4 7AL, United Kingdom and Euratom/UKAEA Fusion Association, Culham Science Centre, Abingdon, Oxfordshire OX14 3DB, United Kingdom

G. Rowlands, T. D. Arber, and N. d'Ambrumenil
Department of Physics, University of Warwick, Coventry CV4 7AL, United Kingdom

(Received 18 September 2002; accepted 30 October 2002)

The Berk–Breizman augmentation of the Vlasov–Maxwell system is widely used to model self-consistent resonant excitation and damping of wave fields by evolving energetic particle populations in magnetic fusion plasmas. The key model parameters are the particle annihilation rate ν_a, which drives bump-on-tail structure, and the linear wave damping rate γ_d. A code, based on the piecewise parabolic method, is used to integrate the fully nonlinear Berk–Breizman system of equations across the whole (ν_a, γ_d) parameter space. The results of this code show that the system's behavior can be classified into one of four types, each of which occurs in a well-defined region of parameter space: chaotic, periodic, steady state, and damped. The corresponding evolution in (x,v) phase space is also examined. © *2003 American Institute of Physics.* [DOI: 10.1063/1.1539854]

I. INTRODUCTION

Containment of the kinetic energy of alpha particles produced in deuterium–tritium reactions is critical to the success of magnetic confinement fusion experiments with burning plasmas. The 3.5 MeV kinetic energy of each fusion-produced alpha particle is required to heat electrons collisionally, which in turn heat deuterium and tritium ions to the temperature required to sustain thermonuclear reactions. Classically, containment of the alpha particles can be achieved if the size of the plasma is large compared to the banana width of trapped alpha particle orbits. However, even if they are initially contained within the plasma, the alpha particles may undergo radial transport as a result of resonant interaction with magnetohydrodynamic (MHD) modes, and in particular modes such as toroidal Alfvén eigenmodes which the alpha particles can themselves excite. A major theoretical and experimental effort is aimed at understanding resonant alpha particle interaction with collective MHD modes.

The Berk–Breizman augmentation of the Vlasov–Maxwell system[1–7] reflects an effort to develop a numerically or algebraically tractable model for the self-consistent interaction between energetic particles and wave fields in fusion plasmas. It can be considered as a generalization of the theory of the electrostatic bump-on-tail instability, and is widely used as a basis for interpreting the interaction of energetic particles with collective modes in tokamak experiments.[4,8–10]

Previous theoretical work has been constrained to particular weakly nonlinear limiting parameter regimes, such as the case of weak damping[5] or slow linear growth,[6,8] and has allowed only particular forms of particle distribution function. For example, the assumption in previous work[5,6] that the bulk of the plasma is cold has meant that it has not been possible to consider the effect of bulk heating by energy transferred from the energetic particle population. Only with a technique that allows investigation across the whole of parameter space can one study the full range of physics that arises from the Berk–Breizman model.

The present work provides, for the first time, numerical solutions to the fully nonlinear set of model equations. By considering the time evolution of the electric field energy, we show that the system behavior can be classified into four types, namely damped, steady state, periodic, and chaotic. Each type of behavior occurs in well-defined regions of parameter space. We present a diagram in parameter space that shows how the model's behavior changes as key parameters are varied. By considering the system's evolution in (x,v) phase space, we also show that the underlying process generic to all parameter values is competition between the formation of the spatially uniform equilibrium distribution and the formation of a phase space hole.

II. THE MODEL EQUATIONS

Throughout this paper we use the following representation of the Berk–Breizman augmentation of the Vlasov–Maxwell system,

$$\mathcal{D}_t f \equiv \partial_t f + v\,\partial_x f + E\,\partial_v f = Q - \nu_a f, \tag{1}$$

$$\partial_t E = -\int v(f - f_0)\,dv - \gamma_d E, \tag{2}$$

where

a)Electronic mail: richard.dendy@ukaea.org.uk

$$f(x,v,t)=\frac{1}{n_0}\times\text{particle number distribution}, \tag{3}$$

$$x=\frac{1}{\lambda_D}\times\text{displacement}, \tag{4}$$

$$v=\frac{1}{v_\theta}\times\text{velocity}, \tag{5}$$

$$t=\omega_p\times\text{time}, \tag{6}$$

$$E(x,t)=\frac{q_s}{m_s v_\theta \omega_p}\times\text{electric field}. \tag{7}$$

Here the Debye length λ_D, the thermal velocity v_θ, and the plasma frequency ω_p satisfy

$$\lambda_D^2=\frac{\epsilon_0 k_B T_s}{n_0 q^2}, \tag{8}$$

$$v_\theta^2=\frac{k_B T_s}{m}, \tag{9}$$

$$\omega_p^2=\frac{n_0 q_s^2}{m_s \epsilon_0}. \tag{10}$$

The quantity T_s does not represent the temperature of the particles (which is not well-defined for a strongly non-Maxwellian distribution) but instead defines a normalizing energy. We work in a spatially periodic box of length L; the spatially averaged distribution function is denoted by $f_0(v)$ in Eq. (2), and the mean number density is n_0. The remaining Berk–Breizman model parameters in Eqs. (1) and (2) are, as usual: the energetic particle source function $Q(v)$, the particle annihilation rate $\nu_a(v)$, and the combined effect, γ_d, of all background damping mechanisms that act on the electric field.

We reduce the number of parameters in the system by rewriting the time evolution equation for the distribution function, Eq. (1), as

$$\mathcal{D}_t f=-\nu_a(f-F_0), \tag{11}$$

where

$$F_0(v)=\frac{Q(v)}{\nu_a}. \tag{12}$$

We note that if $\nu_a>0$, then $f(x,v,t)=F_0(v)$ is the spatially uniform steady state solution of Eq. (11).

Whilst our objective is to study the fully nonlinear system, we must first address the linear stability of the initial distribution. Consider first a small perturbation from this uniform steady state solution $F_0(v)$, and make the ansatz that the perturbed quantities are of the form

$$f_1, E_1 \sim \exp[i(kx-\omega' t)+\gamma' t]+\text{c.c.}, \tag{13}$$

where k, ω', and γ' are all purely real. Linearizing Eqs. (1) and (2), we derive the Landau-type dispersion relation

$$\gamma'+\gamma_d-iw=\int_\Gamma \frac{v\, d_v F_0}{(\gamma'+\nu_a)+i(kv-\omega')}dv, \tag{14}$$

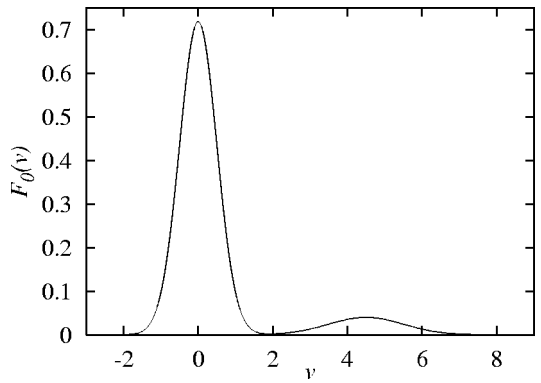

FIG. 1. Bump-on-tail velocity distribution of the form given in Eq. (15), with the parameters that are used in the main simulations described below: $\eta=90\%$, $v_c=1.0$, $v_t=0.5$, and $v_b=4.5$.

where Γ is the appropriate Landau contour. Note that this implicit dispersion relation may have more than one solution for (γ',ω'). We define the *linear growth rate* γ [which is a function of γ_d and ν_a, and depends on the distribution $F_0(v)$] as the most positive γ' (or equivalently the least negative, if the system is damped) for which the linearized dispersion relation Eq. (14) can be satisfied; the frequency corresponding to the growth rate $\gamma'=\gamma$ is denoted by ω. A spatially uniform distribution $F_0(v)$ is considered to be *linearly stable* with respect to small perturbations of the form given in Eq. (13) if the linear growth rate γ is less than zero. For a particular initial distribution $F_0(v)$, we define γ_L to be the linear growth rate that would be possessed by the system in the absence of background damping or particle injection, that is, for the case $\nu_a=\gamma_d=0$.

Motivated by the study of beam-plasma interactions, we choose the initial distribution to be a bump-on-tail distribution of the form

$$F_0(v)=F_{\text{bulk}}+F_{\text{beam}}, \tag{15}$$

where

$$F_{\text{bulk}}=\frac{\eta}{v_c\sqrt{2\pi}}\exp\left(-\frac{1}{2}\left(\frac{v}{v_c}\right)^2\right), \tag{16}$$

$$F_{\text{beam}}=\frac{1-\eta}{v_t\sqrt{2\pi}}\exp\left(-\frac{1}{2}\left(\frac{v-v_b}{v_t}\right)^2\right); \tag{17}$$

an example is shown in Fig. 1. Using Eq. (15), Eq. (11) becomes

$$\mathcal{D}_t f=\nu_a F_{\text{beam}}-\nu_a(f-F_{\text{bulk}}), \tag{18}$$

where the first term on the right-hand side models the effect of energetic particles injected into the system and the second term is mathematically similar to a number conserving collision operator [compare Ref. 12, Eq. (3)].

Berk, Breizman, and co-workers[5,6] have taken the bulk plasma to be cold [$v_c/v_b\to 0$ in Eq. (16)] and the beam to be warm [$v_t/v_b\gg 1$ in Eq. (17)]. In addition, in Refs. 5 and 6, $\nu_a, \gamma \ll \omega$, and ν_a is a function of velocity that acts only on the beam [$\nu_a(v)=0$ for $|v|\ll 1$]. In this case the linearized dispersion relation reduces from the complicated implicit Eq.

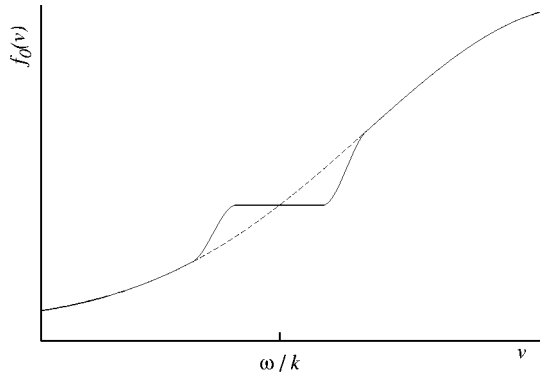

FIG. 2. Plot of a portion of the spatially averaged distribution function $f_0(v)$. The dashed line represents the initial distribution $F_0(v)$; the solid line shows how the distribution flattens as a result of particle trapping.

(14) to a simple explicit algebraic equation, which yields the linearized dispersion relation equations for ω and γ [cf. Ref. 5, Eq. (22)],

$$\omega^2 = \eta, \tag{19}$$

$$2\gamma_L = \pi \omega k^{-2} (\partial_v F_0)_{\omega/k}, \tag{20}$$

$$2(\gamma_L - \gamma) = \gamma_d. \tag{21}$$

Note that in this approximation ω is independent of γ_d and ν_a. As a result, the resonant phase velocity $v_{\rm res} = \omega/k$ and the linear growth rate γ_L depend only on the choice of distribution function $F_0(v)$. Note also that in this approximation γ depends linearly on γ_d and is independent of ν_a. So the linear stability threshold for a particular $F_0(v)$ is the line $\gamma_d = 2\gamma_L$ in (γ_d, ν_a) parameter phase space.

In the fully nonlinear simulations described below, we specify an initial distribution

$$f(x,v,t=0) = (1 + \alpha \cos kx) F_0(v), \tag{22}$$

where $k = 2\pi/L$ and $\alpha \ll 1$ is the amplitude of a small perturbation of the spatially uniform solution $F_0(v)$ defined in Eq. (15). We then compute and study its time evolution. The initial electric field is calculated from Poisson's equation,

$$\partial_x E = \int_{-\infty}^{+\infty} f(v)\, dv - 1 \tag{23}$$

which implies

$$E(x,t=0) = \alpha \cos kx \int_{-\infty}^{+\infty} F_0(v)\, dv. \tag{24}$$

It follows that the system must either oscillate or reach a steady state. Recall the initial conditions given by Eqs. (22) and (24). If the distribution F_0 is linearly stable, then as t increases, $E \to 0$ and $f \to F_0$. If F_0 is linearly unstable, then the electric field and spatial perturbation initially grow exponentially, at a rate defined approximately by the linear growth rate γ obtained from the linearized dispersion relation Eq. (14). This linear phase continues until the spatially averaged distribution function $f_0(v)$ begins to flatten in the velocity region $v \approx \omega/k$, as shown in Fig. 2. This flattening decreases the growth rate of both the electric field and the spatial perturbation. As the effect of the beam drive decreases, the external damping (at a rate γ_d) becomes significant. However, the distribution is being reconstituted at a rate ν_a. These two processes compete. We show in Appendix A that, for positive γ_d and ν_a, the total system energy is bounded. Therefore the wave energy must either oscillate (perhaps nonperiodically) or reach a steady state. Arguing on the basis of energy balance, Berk, Breizman, and Ye[5] show that, in the case of weak damping (γ_d, ν_a small), the system undergoes relaxation oscillations for $\nu_a < \gamma_d$ and saturates to a steady state for $\nu_a > \gamma_d$. Near marginal stability $\gamma \to 0$, Berk, Breizman, and Pekker[6] have developed a perturbative description which allows the oscillation/saturation threshold to be calculated as $\nu = \nu_{\rm cr} \equiv 4.38\gamma$.

While the weak damping and marginal stability results provide a valuable guide to some aspects of the system's behavior, no quantitative description has previously been obtained to describe the system's fully nonlinear behavior over large regions of (γ_d, ν_a) space. In the present work, we provide a quantitative treatment that can be applied to Eqs. (1) and (2) for any choice of initial velocity distribution $F_0(v)$ and across the whole of (γ_d, ν_a) parameter space.

III. NUMERICAL METHOD

Our numerical algorithm for the solution of Eqs. (1) and (2) relies on combining the methods of Strang splitting[13] and the piecewise parabolic method.[15] It is a logical development of the method of Cheng and Knorr;[14] a full account is given in Arber and Vann.[11]

We write Eqs. (1) and (2) in the form

$$\partial_t Z = \sum_{j=1}^{4} Y_j[Z], \tag{25}$$

where the vector $Z = (f, E)$ and

$$Y_1[Z] = (-v\, \partial_x f,\ 0), \tag{26}$$

$$Y_2[Z] = (Q - \nu_a f,\ 0), \tag{27}$$

$$Y_3[Z] = \left(0,\ -\int v(f - f_0)\, dv - \gamma_d E\right), \tag{28}$$

$$Y_4[Z] = (-E\ \partial_v f, 0). \tag{29}$$

We can then apply the Strang splitting formula,

$$\Phi_Y^t[Z_0] = \Phi_{Y_1}^{(1/2)\,t} \circ \Phi_{Y_2}^{(1/2)\,t} \circ \Phi_{Y_3}^{(1/2)\,t} \circ \Phi_{Y_4}^{t} \circ \Phi_{Y_3}^{(1/2)\,t} \circ \Phi_{Y_2}^{(1/2)\,t} \circ \Phi_{Y_1}^{(1/2)\,t}[Z_0] + \mathcal{O}(t^3), \tag{30}$$

where the flow operator Φ is defined by

$$\{\partial_t Z = Y[z] \text{ and } Z(t=0) = Z_0\} \Rightarrow Z(t) = \Phi_Y^t[Z_0] \tag{31}$$

and the composition $V \circ W(x) \equiv V(W(x))$.

We note that each of the operators Y_j modifies only one of f and E. Consequently it is possible to solve exactly for Y_2 (at constant E) and Y_3 (at constant f). We are then left with two equations of the form,

$$\partial_t U + c\, \partial_\xi U = 0, \tag{32}$$

where c is independent of U and ξ. These advection equations are solved via the piecewise parabolic method.[15] This method is monotonicity preserving and does not accentuate already existing extrema. It has been shown[11] that this method performs well as the advection component of this Vlasov-solving algorithm. We note that flux conservative schemes such as the piecewise parabolic method do not have a stability condition on the Courant number $\lambda=\Delta t/c\Delta\xi$ of the form $\lambda<\lambda_c$. However, as we describe below, one might wish to impose a condition on the maximum value that the Courant number is permitted to attain, of the form $\lambda<\lambda_{\max}$ in the interests of accuracy.

IV. CHOICE OF MODEL PARAMETERS

The physical parameters of the model one would like to study coupled with considerations concerning numerical feasibility determine a sensible choice of coding parameters. An example is phase space resolution; it is important to use a sufficient number of grid points so that important structures are reproduced accurately, but one must not use too many grid points, otherwise the required computer time is unnecessarily large.

Few particles in the beam (hence large η) and a large beam temperature (large v_t/v_b) imply a small linear bump-on-tail drive $\gamma_L\propto(\partial_v F_0)_{\omega/k}$. As a result, the width of the region in velocity space over which the distribution function is flattened is small, as is the amplitude of any wave mode. It is numerically problematic that the qualitative nature of the system's behavior depends on $(\partial_v f)_{v=\omega/k}$: since any numerical scheme is dissipative, it causes regions of the distribution that are flattened because of particle trapping to possess a gradient which is nearer than it should be to the gradient of the surrounding distribution. In particular, in the bump-on-tail problem this effect can cause a steady state system to acquire an artificial linear drive. A cold bulk (with small v_c) has a similar numerical problem—specifically that numerical diffusion causes artificial heating of the bulk.

The initial distribution parameters in Eqs. (16), (17), and (22) are chosen as $\eta=90\%$, $v_c=1.0$, $v_t=0.5$, $v_b=4.5$, $\alpha=1\%$. This velocity distribution is plotted in Fig. 1. We show in Appendix B that, for this choice of initial distribution, the system is restricted to $|v|<v_{\max}=8$ (indicated by particle conservation to within one part in 10^{12}) and that $N_x=128$ points in x, with corresponding grid spacing $\Delta x=L/128$, and $N_v=1025$ points in v, with grid spacing $\Delta v=2v_{\max}/N_v$, are sufficient to capture the system's structure. We have also chosen the timestep at each time to be the largest such that $\Delta t\leq 0.1$ and the Courant number $\lambda\leq\lambda_{\max}=3$.

If the electric field is very small, the particles are *free streaming*: they experience phase space advection only in the x-direction. Therefore the phase space line $v=v_j$ keeps recovering the same state with period $T=L/v_j$. Since we are working on a discrete uniform Eulerian grid, the system then develops an unphysical temporal periodicity under this spatial advection: the phase space lines are regularly spaced at a distance Δv, so the entire grid is periodic with the period $T_R\equiv L/\Delta v$ (i.e., the period of the phase space line with smallest nonzero $|v|$). This phenomenon is known as *recurrence* and T_R is called the *recurrence time*. Note first that recurrence only occurs when the particles are free streaming. This is the case when the advection in the v-direction is small compared to the advection in the x-direction so that $\overline{E}\,T_R\lesssim\Delta v$, where $\overline{E}$ is some measure of the average electric field amplitude. Second, the addition of distribution reconstitution to the Vlasov equation gives our system a finite memory of length $\sim\nu_a^{-1}$. So, given our other choices of numerical parameters, we have a recurrence time $T_R=1344\,\omega_p^{-1}$, while the numerics will only show this recurrence if $\overline{E}\lesssim 5\times10^{-5}$ and $\nu_a\lesssim 2\times10^{-3}$. Detailed benchmarking for the choice of numerical parameters is described in Appendix B.

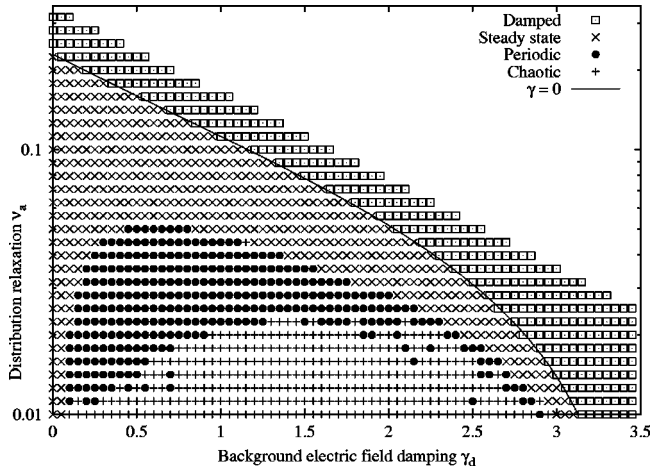

FIG. 3. Characterization of the behavior of the Berk–Breizman system across the entire (γ_d,ν_a) parameter space; note the logarithmic scale on the vertical ν_a axis. The four types of behavior occur in well-defined regions of the parameter space. The solid line is the linear stability threshold, computed numerically directly from the dispersion relation Eq. (14); the damped-to-steady-state border agrees well with this calculation, which confirms that recurrence is not a significant effect.

The simulations were performed on a cluster of 1.4 GHz PCs; MPI was used for efficient load sharing between nodes. A simulation with an end time of $t=3000\,\omega_p^{-1}$ takes approximately 90 min on a single processor. On a 32 node cluster, this enables, for example, the 1405 simulations required for the generation of Fig. 3 below to be performed in less than 3 days. As recently as 1997 a single simulation of this length would have been described as ''very long'' in the literature.[16]

V. RESULTS: CHARACTERIZATION OF BEHAVIORS

We choose a quantity that reflects the state of the system described by Eqs. (1) and (2), compute its evolution with time, and characterize the resultant time series. The quantity we have chosen is the spatially averaged electric field energy density,

$$A(t)=\frac{1}{L}\int_0^L E(x,t)^2dx. \tag{33}$$

As we shall see, one can categorize the behavior of A with time t as being in one of four categories in the limit $t\to\infty$:

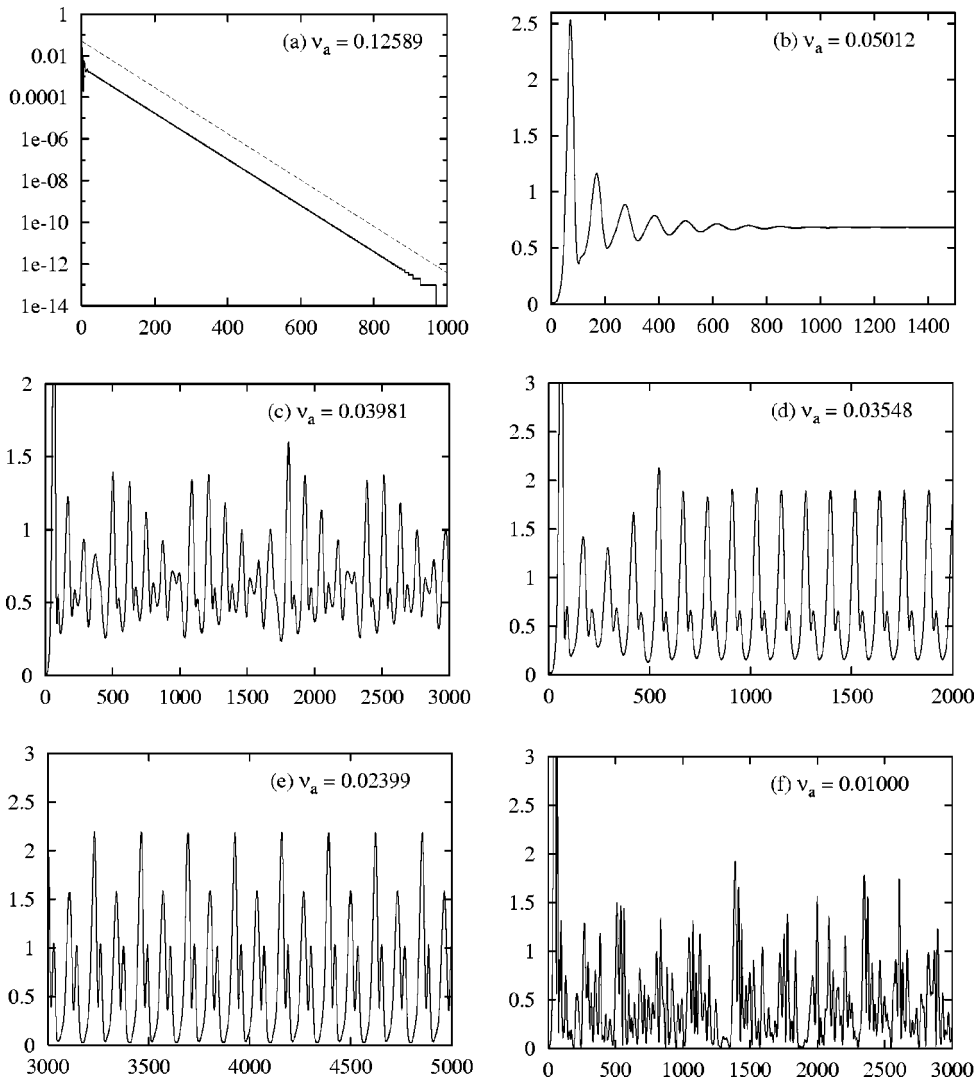

FIG. 4. Different phenomenological regimes of the Berk–Breizman model are represented here by plots of electric field energy $A(t)$ ($\times 10^3$) versus time t. In each plot, the background electric field damping $\gamma_d = 1.0$; the particle injection rate ν_a is decreased as we proceed through the plots (a)–(f).

(1) Damped: $A(t) \to 0$;
(2) Steady state: $A(t) \to A_\infty > 0$;
(3) Periodic: there exists $T > 0$ such that $A(\tau + T) \to A(\tau)$ for all $\tau \in [t, t+T]$;
(4) Chaotic: A is bounded, but does not fall into one of the previous categories.

We show in Appendix A that, for $\nu_a, \gamma_d \neq 0$, the total system energy is bounded. This implies that $A(t)$ is also bounded and therefore that the list of categories for $A(t)$ is complete. We note that it is possible that the system might display nonperiodic bounded behavior that is phase space filling and yet is not chaotic; motion on a torus for irrational winding number is of this type. To distinguish between these two types of behavior, it is helpful to study the Lyapunov spectrum of the system: specifically, chaos requires that nearby trajectories diverge, or equivalently, that there exists at least one positive Lyapunov exponent. Application of the method of Rosenstein *et al.*[17] indicates that, for parameter values (γ_d, ν_a) that produce nonperiodic behavior, there exists a positive Lyapunov exponent and therefore the system is indeed chaotic.

Appendix C describes how we categorize the time series into one of these four types.

We have performed runs of length $3000\omega_p^{-1}$ in the parameter region $0 \leqslant \gamma_d < 3.5$, $0.01 \leqslant \nu_a < \nu_{\max}$, where $\nu_{\max} = \min(0.35, \exp(-\gamma_d))$ is chosen to be above the linear stability threshold as computed by direct numerical solution of the dispersion relation Eq. (14). The computed behavior of the fully nonlinear Berk–Breizman system [Eqs. (1) and (2)] can then be characterized across the whole of (γ_d, ν_a) parameter space as shown in Fig. 3. We remark that previous work applies only near the origin $\nu_a = \gamma_d = 0$ or near the linear stability threshold $\gamma = 0$. Both regimes are relevant to present day experiments and therefore so is the intervening region. We note that the four types of behavior are principally restricted to well defined regions in parameter space, although there are some outliers, primarily on the borders of

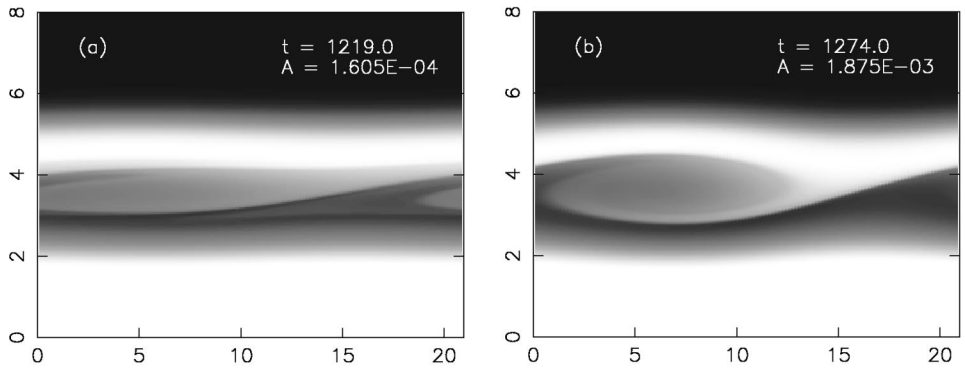

FIG. 5. Plots of the distribution function in (x,v) phase space. The portion of the plot for $v<0$ is omitted. These figures show the distribution function at the extreme values of $A(t)$ for the point in parameter space $(\gamma_d,\nu_a)=(1.000,0.03548)$, which lies within the periodic regime. There is the bulk dense plasma for $|v|\lesssim 2$. (a) shows the distribution when the electric field energy $A(t)$ is at a minimum. The plasma is quite homogenous and few particles are trapped. In (b), $A(t)$ is at a maximum; A has increased by a factor of 10 from (a). A large number of particles are trapped in the phase space hole.

the periodic region. These points are a result of the numerical limitations placed on time series correlation outlined towards the end of Appendix C. One can reasonably conjecture that the regions are simply connected and that this would be shown by longer computations. The agreement between the linear stability threshold computed directly from the dispersion relation Eq. (14) (displayed as a solid line) and the damped-to-steady-state boundary tends to confirm our argument that recurrence does not have a significant effect. To illustrate the bifurcation path and examples of the four types of behavior, we have taken a cut along a vertical line in parameter space at $\gamma_d=1$; representative plots are shown in Figs. 4(a) to 4(f) for decreasing values of ν_a.

(a) For large ν_a, the fully nonlinear solution (solid line) exhibits damped behavior. The electric field energy $A(t)$ goes to zero with a well-defined decay rate. (We again note that there is no recurrence effect.) The dashed line represents the corresponding approximate dispersion relation solution $\gamma=-0.0128$ from Eq. (14); we note that there is good agreement between the fully nonlinear solutions and the linear analytical approximation.

(b) As ν_a is reduced, $A(t)$ initially grows exponentially. and then saturates at some nonzero value. The example here is underdamped in the sense that it continues to oscillate many times about the saturation value. Both overdamped and critically damped cases also occur.

(c) As ν_a is further decreased, the system enters a transitional regime where it is difficult to classify the behavior.

(d) The system enters a broad region of periodic behavior. Periodic orbits of this system seem often to feature pairs of peaks—a large peak followed by a smaller peak.

(e) At still lower ν_a, the system goes through a complex set of bifurcations on the path to chaos. The first bifurcation (shown here) would appear to be the first of a period doubling sequence, as proposed by Heeter *et al.* (Ref. 9). However, preliminary results from much longer runs across a small cut in parameter space suggest that this is not the case.

(f) As ν_a is further reduced, the system becomes chaotic. That the Berk–Breizman system possesses a chaotic regime reinforces the earlier conjecture (made on the basis of a multiple scales argument) that such a regime exists.[6] However, a quantitative analysis of our results shows that the chaos is not the sort of avalanching chaos observed in the numerical simulations of Berk, Breizman, and Pekker.[7] The chaotic regime is extensive in parameter space; it is observed for a broad range of γ_d but only for weak ν_a (see Fig. 3).

The temporal evolution of the distribution function $f(x,v,t)$ in (x,v) phase space is shown in Fig. 5 by two snapshots of f taken when the system is in its periodic phase with $(\gamma_d,\nu_a)=(1.000,0.03548)$. The snapshots are taken at the minimum and maximum values of the electric field energy $A(t)$, which differ by a factor of 10 between the two pictures. We note that small A corresponds to a largely uniform distribution, whilst large A corresponds to significant spatial structure in (x,v) phase space. Moreover, the structure is a particle phase space hole: particles are trapped in the potential of the electric field wave mode. The wave mode, and the phase space hole, have a characteristic velocity which can be read off the velocity axis [the phase of the pictures shown here has been shifted for clarity so that the maximum value of the electric field $E(x,t)$ occurs at the edge of the plots].

One may also perform simulations for different shapes

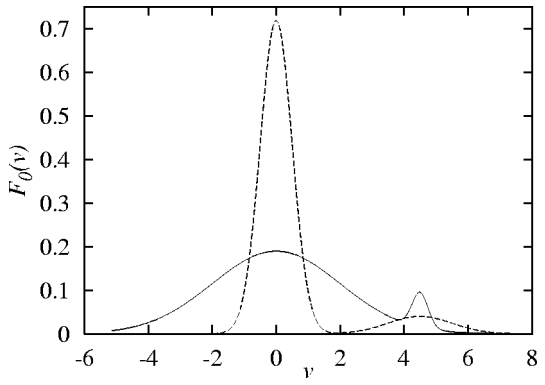

FIG. 6. Alternative bump-on-tail distributions. The warm beam distribution ($\eta=90\%$, $v_c=0.5$, $v_t=1.0$) is plotted as the dashed line, and the warm bulk distribution ($\eta=95\%$, $v_c=2.0$, $v_t=0.5$) as the solid line. In both cases (as before) the mean beam velocity $v_b=4.5$.

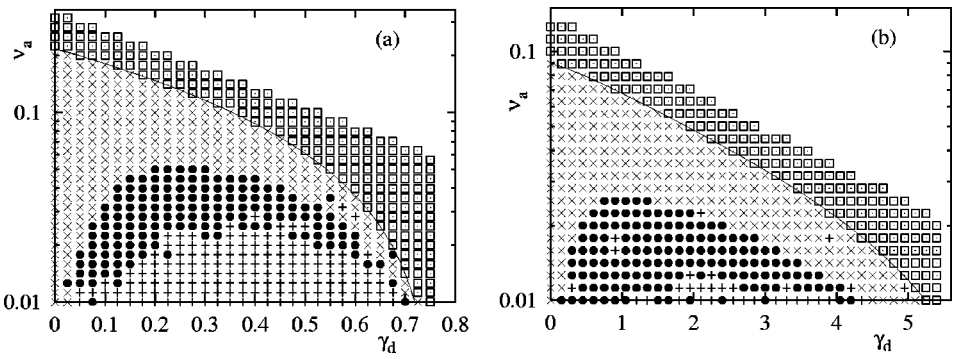

FIG. 7. Classification of the behavior found in (γ_d, ν_a) parameter space for the alternative initial distributions of Fig. 6: (a) warm beam; (b) warm bulk. (For the symbol key, please refer to Fig. 3.) There is strong similarity between these two categorization diagrams and that shown in Fig. 3, suggesting that the bifurcation path is robust to changes in the initial distribution. The small beam gradient (in the warm beam case) and the small beam width (in the warm bulk case) is likely to cause the numerical results to be slightly less accurate.

of bump-on-tail distribution. Two further examples we have investigated are shown in Fig. 6, namely a warm beam distribution and a warm bulk distribution. The corresponding phenomenology of the Berk–Breizman system is shown in Fig. 7.

VI. CONCLUSION

In this paper, we have shown that current numerical techniques and computer resources make it possible to generate accurate solutions for the fully nonlinear Berk–Breizman augmentation of the Vlasov–Maxwell system. For the first time, the full range of (ν_a, γ_d) parameter space has been explored, and the corresponding system behavior categorized. Physical understanding is aided by the deployment of numerical diagnostics in (x,v) space, as well as for the time dependence of field amplitude. A new chaotic regime for field amplitude evolution has been rigorously identified, and its boundaries established. Where appropriate, our results confirm, and are benchmarked by, earlier results in specific limiting parameter regimes that were obtained using analytical approximations. The successful track record of analytical solutions of the Berk–Breizman system in assisting interpretation of experimental observations of interacting energetic particle populations and MHD modes in tokamaks is well known. We anticipate that access to fully nonlinear solutions of this system over a greatly extended parameter range, gained from the present work, will lead to further interpretive developments.

ACKNOWLEDGMENTS

The authors would like to thank Professor Boris Breizman and Professor Herb Berk for helpful discussions.

This work was supported in part by Euratom, the UK DTI, EPSRC and the Leverhulme trust.

APPENDIX A: TO SHOW THAT THE TOTAL SYSTEM ENERGY IS BOUNDED

The spatially averaged mean total energy density in the system is $H=T+A$, where the kinetic contribution is given by

$$T(t)=\frac{1}{L}\int_0^L\int_{-\infty}^{+\infty} v^2 f(x,v,t)\; dv\; dx \tag{A1}$$

and $A(t)$ is the spatially averaged electric field energy defined by Eq. (33). The rate of change of H follows from the corresponding moments of Eqs. (1) and (2) and is given by

$$d_t H = K - \nu_a T - 2\gamma_d A \tag{A2}$$

$$\leqslant K - \min(\nu_a, 2\gamma_d)\, H. \tag{A3}$$

Here $K \geqslant 0$ is a constant determined by the injection distribution [see Eq. (18)]. It follows that

$$H > H_{\max} \equiv \frac{K}{\min(\nu_a, 2\gamma_d)} \Rightarrow d_t H < 0. \tag{A4}$$

So, for $\nu_a > 0$ and $\gamma_d > 0$, an upper bound on the total energy exists.

APPENDIX B: BENCHMARKING

To test whether our choice of coding parameters is appropriate, we have performed runs at a number of different values of the physical parameters (γ_d, ν_a) for various choices of the numerical parameters N_v, N_x, $\Delta t_{\max}$. In this section we display the results for one particular parameter value. This point $(\gamma_d, \nu_a) = (3.1, 0.01)$ in parameter space is chosen because it is close to the boundary between two regions of different qualitative behavior [in this case near the linear stability threshold $\gamma = 0$ as computed from the dispersion relation Eq. (14)], and a prime concern is that the choice of coding parameters should not govern the qualitative nature of the system's behavior or the bifurcation path in parameter space. We remark that the condition for the robustness of the categorization diagram Fig. 3 is much less stringent than the condition for the quantitative convergence of time series. We refer to the results shown in Fig. 8.

(a) Varying the velocity space resolution. At $N_v = 257$, recurrence effects dominate and the wrong qualitative behavior is produced. At $N_v = 513$, the correct qualitative behavior is recovered, but there is still significant quantitative error. As N_v is further increased, the time series converges quantitatively at the resolution of the graphical plot.

(b) Varying the temporal and spatial resolutions. We find that neither an increase in $\Delta t_{\max}$ (corresponding to an increase in $\lambda_{\max}$) nor an increase in the number of points in x space leads to a significant quantitative change in $A(t)$. We infer that our choices of $\Delta t_{\max} = 0.1$ and $N_x = 128$ provide sufficiently high resolution for convergence.

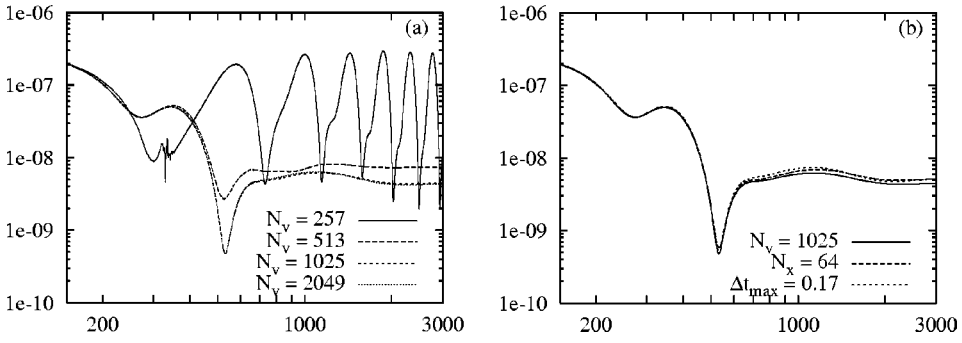

FIG. 8. Time series $A(t)$ for physical parameters $(\gamma_d, \nu_a)=(3.1,0.01)$ and various coding parameters. (a) We vary N_v and observe quantitative convergence (at the resolution of the plot) at $N_v=1025$. (b) We lower the resolution in both time and space and observe no significant quantitative change in solution. Again we infer convergence.

For points (γ_d, ν_a) far from category boundaries, we find even better quantitative agreement for the time series generated.

APPENDIX C: NUMERICAL CATEGORIZATION OF TIME SERIES

In the analysis we consider a time window $0<t_{\min}<t_{\max}$, with $A(t)$ sampled with a period Δt (which may be larger than the computational time step). The objective is to choose $t_{\min}$ sufficiently large that transient behavior has died out before the start of the analysis time window. We note that this is not always possible to guarantee and discuss below the impact of this difficulty on categorization. We have $t_{\max}-t_{\min}=(N-1)\Delta t$ for some positive integer N so that we have N data points $A_j=A(t_{\min}+j\Delta t)$, where $j\in[0,N-1]$. Then we can define:

(i) The mean value $\langle A\rangle=\Sigma_{j=0}^{N-1}A_j/N$;
(ii) The global minimum $A_{\min}=\min_j\{A_j\}$ and maximum $A_{\max}=\max_j\{A_j\}$;
(iii) The set labeling local minima $S_{\min}=\{j\in\mathbb{N}:A_j<\min\{A_{j\pm1}\}\}$, and similarly $S_{\max}$.

For any $0<j\leqslant N/2$, we define the correlation window length N_j to be the largest integer such that $N_j\leqslant N/j$ and the window function by $B_i=A_l-\langle A\rangle$, where $l=N-(i \bmod N_j)$. We then write the two point correlation function as

$$R_j=\left(\sum_{i=0}^{N_j-1}B_iB_{i+j}\right)\Big/\left(\sum_{i=0}^{N_j-1}B_i^2\right). \tag{C1}$$

The overall correlation $R=\max_j\{R_j\}$. We save time in the computation of R by making the assumption that R_j will be large only when j corresponds to the time difference between local extrema. We have chosen $t_{\min}=1000\,\omega_p^{-1}$, $t_{\max}=3000\,\omega_p^{-1}$, and $\Delta t=0.5$. We then proceed through the following decision tree:

(1) IF $\langle A\rangle<\epsilon_1=10^{-12}$ THEN *damped*
(2) ELSE IF $A(t)$ is monotonic AND $(A_{\max}-A_{\min})/\langle A\rangle<\epsilon_2=5\%$ THEN *steady state*
(3) ELSE IF $A(t)$ is monotonically decreasing THEN-*damped*
(4) ELSE IF
   (a) the system is oscillating about a value to which it is tending (i.e., for all $i>j$, $(i,j\in S^{\min}\Rightarrow A_i<A_j)$ AND $(i,j\in S^{\max}\Rightarrow A_i>A_j)$), OR
   (b) $(A_{\max}-A_{\min})/\langle A\rangle<\epsilon_3=1\%$, OR
   (c) $(A_{\max}-A_{\min})<\epsilon_4=10^{-9}$

THEN *steady state*
(5) ELSE IF $R>1-\epsilon_5=75\%$ THEN *periodic*
(6) ELSE IF number of extrema is not less than four THEN *nonperiodic*

We note that this decision tree cannot correctly classify periodic behavior if the period is greater than half the length of the sampling window—it is either classified as nonperiodic or not classified at all. Similarly, working with simulations of finite time, we cannot guarantee that the system will not at some later time settle down to a periodic orbit, for example. Given more computer time, one could run longer simulations and increase the threshold correlation value. As a result, the choice of correlation threshold is the most difficult to make. The behavior of the system on the border of the periodic region is complicated, as discussed above, and we are subject to both the numerical issues just outlined.

[1] H. L. Berk and B. N. Breizman, Phys. Fluids B **2**, 2226 (1990).
[2] H. L. Berk and B. N. Breizman, Phys. Fluids B **2**, 2235 (1990).
[3] H. L. Berk and B. N. Breizman, Phys. Fluids B **2**, 2246 (1990).
[4] H. L. Berk, B. N. Breizman, and H. Ye, Phys. Rev. Lett. **68**, 3563 (1992).
[5] H. L. Berk, B. N. Breizman, and H. Ye, Phys. Fluids B **5**, 3217 (1993).
[6] H. L. Berk, B. N. Breizman, and M. Pekker, Phys. Rev. Lett. **76**, 1256 (1996).
[7] H. L. Berk, B. N. Breizman, and M. Pekker, Phys. Plasmas **2**, 3007 (1995).
[8] A. Fasoli, B. N. Breizman, D. Borba, R. F. Heeter, M. S. Pekker, and S. E. Sharapov, Phys. Rev. Lett. **81**, 5564 (1998).
[9] R. F. Heeter, A. F. Fasoli, and S. E. Sharapov, Phys. Rev. Lett. **85**, 3177 (2000).
[10] K. L. Wong, R. Majeski, M. Petrov, J. H. Rogers, G. Schilling, J. R. Wilson, H. L. Berk, B. N. Breizman, M. Pekker, and H. V. Wong, Phys. Plasmas **4**, 393 (1997).
[11] T. D. Arber and R. G. L. Vann, J. Comput. Phys. **180**, 339 (2002).
[12] P. L. Bhatnagar, E. P. Gross, and M. Krook, Phys. Rev. **94**, 511 (1954).
[13] G. Strang, SIAM (Soc. Ind. Appl. Math.) J. Numer. Anal. **5**, 506 (1968).
[14] C. Z. Cheng and G. Knorr, J. Comput. Phys. **22**, 330 (1976).
[15] P. Colella and P. R. Woodward, J. Comput. Phys. **54**, 174 (1984).
[16] G. Manfredi, Phys. Rev. Lett. **79**, 2815 (1997).
[17] M. T. Rosenstein, J. J. Collins, and C. J. De Luca, Physica D **65**, 117 (1993).